Modeling spontaneous chiral symmetry breaking and deracemization phenomena: Discrete versus continuum approaches

Celia Blanco
Department of Chemistry and Biochemistry, University of California, Santa Barbara, California 93106-9510, USA

Josep M. Ribó
Department of Organic Chemistry, and Institute of Cosmos Science (IEEC-UB), University of Barcelona, c. Martí i Franquès 1, 08028 Barcelona, Catalonia, Spain

David Hochberg*
Centro de Astrobiología (CSIC-INTA), Carretera Ajalvir Kilómetro 4, 28850 Torrejón de Ardoz, Madrid, Spain
(Received 8 October 2014; published 2 February 2015)

We derive the class of population balance equations (PBE), recently applied to model the Viedma deracemization experiment, from an underlying microreversible kinetic reaction scheme. The continuum limit establishing the relationship between the micro- and macroscopic processes and the associated particle fluxes erases the microreversible nature of the molecular interactions in the population growth rate functions and limits the scope of such PBE models to strict kinetic control. The irreversible binary agglomeration processes modeled in those PBEs contribute an additional source of kinetic control. These limitations are crucial regarding the question of the origin of biological homochirality, where the interest in any model lies precisely in its ability for *absolute asymmetric synthesis* and the amplification of the tiny inherent statistical chiral fluctuations about the ideal racemic composition up to observable enantiometric excess levels.

DOI: 10.1103/PhysRevE.91.022801 PACS number(s): 82.20.−w, 82.40.Bj, 05.70.Ln, 05.60.Cd

I. INTRODUCTION

In chemistry, absolute asymmetric synthesis or spontaneous mirror symmetry breaking (SMSB) refers to the transformation of achiral or racemizing initial products to chiral reaction products in detectable enantiomeric excesses, and in the absence of any chiral polarization. This may occur in enantioselective-autocatalytic reaction networks leading to a bifurcation scenario [1], i.e., if the racemic state is metastable and the stable state (steady state of minimum entropy production) is one of the two degenerate chiral branches. This is achieved by virtue of the chiral fluctuations generated by the inherent statistical fluctuations around the ideal racemic composition [2]. In the framework of linear thermodynamics of irreversible processes, this mirror symmetry breaking occurs for specific system parameters and only in the case in which the system cannot come into thermodynamic equilibrium with its surroundings [3]. However, in this latter case, such reaction networks may yield kinetically controlled absolute asymmetric synthesis, i.e., temporary, but synthetically useful, enormous amplifications of the extremely tiny enantiomeric excesses generated by chiral fluctuations up to detectable enantiomeric excess values [4]. The Soai reaction [5] is a well-established experimental proof of this. The significance of studying these systems is due to the topic of biological homochirality which, in our opinion, is a central point for the design of potential systems mimicking primordial processes of life. In this respect, such studies should be performed within the framework of linear thermodynamics of irreversible processes [6], since this is the appropriate scenario for describing most of the chemical reactions in primordial organisms implying enantioselective transformations.

A key point is that the principle of detailed balance (known as the principle of microreversibility in chemistry) applies in both equilibrium and in linear irreversible thermodynamics scenarios. This implies that, in a dynamic and kinetic modeling of the system, the matter flow in the material transformations must necessarily be described by forward and reverse rates whose ratios are in strict compliance with the corresponding free-energy differences for the chemical species involved in that specific transformation. In models and simulations where microreversibility (detailed balance) is not taken into account, artifactual SMSB may be erroneously obtained and misinterpreted.

An intriguing experimental scenario of absolute asymmetric synthesis is that first reported by Viedma on the deracemization of racemic enantiopure crystal mixtures, the so-called racemic conglomerates [7] of achiral or fast racemizing compounds. The experimental setup involves the continuous wet mechanical grinding of a racemic conglomerate mixture of enantiomorphic crystals [8]. The theoretical understanding of Viedma's experiment is as yet an unsettled matter [9]. Nevertheless, the indisputable nexus of agreement between all experimental and theoretical reports to date is that the higher solubility of the smaller crystals (the Gibbs-Thomson effect) [10] obtained through grinding creates a supersaturated media for the larger crystals, and that a steady-state continuous distribution of visible crystal sizes and small crystal clusters down to the monomer must be obtained.

Among the many models proposed attempting to explain Viedma deracemization [9], population balance equations (PBEs) have begun to be applied recently [11,12]. Prior to this, population balance methods have been used successfully for modeling crystallization processes [13]. The PBEs applied

*hochbergd@cab.inta-csic.es

to *achiral* crystallizations are based on a description of crystal growth processes from the first nucleating particles up to the large crystals. They mostly deal with the crystal growth of single species or to selective crystallization of different compounds. Specific attempts to use PBEs for describing the Viedma phenomenon are reported using profiles of the energy differences between clusters/crystals by the description of the critical size cluster through the supersaturation value given by the classical primary nucleation theory [11]. However, in such population balance modeling, only *net* growth and dissolution flows, according to whether the cluster/crystal size is above or below the critical size cluster, are considered, and the conclusion drawn from these studies is that small initial differences between enantiomorphs, for example in crystal size distributions, are the origin of the final chiral outcome, i.e., it is a controlled process [11], but moreover that the final stable state must be chiral [11]. We analyze below the same general class of PBEs, but under the fundamental thermodynamic constraints dictated by microreversibility (i.e., detailed balance in physics).

By means of a reversible kinetic scheme, we established recently that the Viedma experiment corresponds to a genuine SMSB bifurcation scenario [14]. To accomplish this, it was necessary to recognize the basic trends of the aggregation/deaggregation network in the Viedma phenomenon, taking into account the thermodynamic constraints implied by the interacting processes (mechanical attrition, solubilization, crystal growth, and racemization). Careful consideration was given to forward and reverse reaction rates in all the processes. Mechanical grinding of clusters is the only process that is genuinely irreversible. The needed mutual inhibition step is to be found in the *reverse flow* of chiral clusters toward the racemizing monomers in solution. That is, the symmetry-breaking bifurcation depends sensitively on the microflow (detailed balance) of chiral matter back to solution where it can racemize, becoming available for further growth of clusters.

In view of the above, the following question then arises: What relation is there between the microreversible kinetic reaction schemes [14] and the continuum population balance models [11,12] applied to Viedma deracemization? They are actually two complementary sides of the same coin. In this paper, we will start from the general discrete kinetic scheme employed in [14], namely (i) racemizing chiral monomers in solution, (ii) monomer-cluster growth and dissolution, (iii) cluster-cluster agglomeration and fragmentation, and (iv) irreversible breakage of clusters, and we *derive*, by means of the continuum limit, the *general class* of PBEs that have been applied to the Viedma deracemization phenomenon. This demonstration not only serves to bridge the two approaches, but it also brings to the fore the important issue of micro- versus macrofluxes in the context of chiral *bifurcation* phenomena and deracemization. We establish a mathematical connection between discrete microreversible kinetic rate schemes and the continuous differentiable variables and particle population distribution functions employed in the PBEs, identifying the advective fluxes, Eq. (2), as well as the growth/dissolution functions that are implied by them. This provides a first-principles microscopic reason for these semiempirical continuous growth rate terms, and it also reveals clearly at what stage the microreversibility/detailed balance is permanently washed out in taking the *continuum limit*. We also derive continuum agglomeration and fragmentation terms [i.e., the h terms above in Eq. (1)] from an underlying *reversible* microscopic description. This establishes that the cluster-cluster agglomeration terms employed in the specific PBE models [11,12] represent *irreversible* cluster-cluster agglomerations, and are thus an additional source of (undesired) kinetic control.

II. POPULATION BALANCE MODELING

Briefly, the objective in population balance modeling is to calculate the particle distribution or density function $f(\boldsymbol{x},\boldsymbol{r},t)$, where the vector $\boldsymbol{x}$ denotes a collection of different internal quantities or attributes (e.g., size, mass, internal composition, age, etc.) associated with the solid phase particles, and $\boldsymbol{r}$ denotes the particle position vector in physical space. This distribution function is obtained as a solution of the general population balance equation [15]:

$$\frac{\partial f}{\partial t} + \nabla_x \cdot (\boldsymbol{J_x}) + \nabla_r \cdot (\boldsymbol{J_r}) = h(\boldsymbol{x},\boldsymbol{r},t), \tag{1}$$

where

$$\begin{aligned} \boldsymbol{J_x} &= f(\boldsymbol{x},\boldsymbol{r},t)\dot{\boldsymbol{X}}(\boldsymbol{x},\boldsymbol{r},\boldsymbol{C},t), \\ \boldsymbol{J_r} &= f(\boldsymbol{x},\boldsymbol{r},t)\dot{\boldsymbol{R}}(\boldsymbol{x},\boldsymbol{r},\boldsymbol{C},t), \end{aligned} \tag{2}$$

are the bulk advective *particle fluxes* [16] through internal coordinate space ($\boldsymbol{x}$) and through physical space ($\boldsymbol{r}$), respectively: that is, the number of particles flowing per unit time per unit area normal to the direction of the generalized velocity vectors $\dot{\boldsymbol{X}}$, and $\dot{\boldsymbol{R}}$. These velocities or rates of change may also depend on the continuous phase vector $\boldsymbol{C}$, including all the continuous background quantities that might affect the behavior of the particles (e.g., chemical concentrations, supersaturation, background fluid flow, etc.). $\boldsymbol{C}$ satisfies its own standard transport equation. The term $h(\boldsymbol{x},\boldsymbol{r},t)$ represents all birth and death processes in the solid phase, such as particle agglomeration and particle fragmentation. Models must be provided for these rates of change $\dot{\boldsymbol{X}}$ and $\dot{\boldsymbol{R}}$ as well as for h if agglomeration and or fragmentation are to be included. Equation (1) can then be solved in principle when the initial and boundary conditions are provided.

While the PBE approach Eq. (1) may be satisfactory for modeling features of standard single-species crystallization [17,18], it is not obviously suitable to apply it, without prior careful consideration, to *bifurcation* phenomena, such as spontaneous mirror symmetry breaking (SMSB), which involves a pair of *energetically degenerate competing enantiomers*. This is because the underlying PBE formalism itself [15], which is based on the Reynolds transport theorem, is articulated in terms of bulk system particle (macro)fluxes, Eq. (2), which can be oblivious to the delicate constraints dictated by thermodynamics (e.g., detailed balance). In contrast to microscopic kinetic schemes, which aim at modeling individual reactions, population balance modeling is more akin to a *"global"* approach based on coarse-grained (low spatial resolution) variables and parameters. It treats entire populations rather than individual particles. The microscopic resolution of the underlying molecularity or detail can be lost at the level of the population balance model. This loss of resolution is a consequence of the continuum limit that

one implicitly (or explicitly) takes in going from the fine- to the coarse-grained system variables and parameters. The PBE models applied to the Viedma experiment [11,12] involve net growth or net dissolution flow for clusters above and below the critical size nucleus, respectively. Thus the principle of microreversibility is obscured in the choice of PBE system parameters, and the simulations based on those functions can and do yield artifactual SMSB. Moreover, the inclusion of homochiral cluster-cluster agglomeration, via the h-term in Eq. (1), should be a microreversible process as well. But the inverse process, namely deagglomeration or binary fragmentation (not to be confused with mechanical grinding, which is a totally irreversible process), is lacking in the models proposed so far [11,12]. This omission yields a further source of (undesired) kinetic control.

There is an important practical advantage from relating the kinetic rate and population balance approaches. Because PBE's are expressed in terms of derivatives of growth rates and particle distribution functions and involve integrals over complicated kernels, analytic solutions are hard to come by and one must frequently resort to numerical simulation. Simulations of PBEs, Eqs. (1) and (2), in turn, require implementing some discretization method [15], and one is often led to numerically integrating sets of coupled ordinary differential equations, just as for direct simulations of kinetic reaction rate schemes. However, the mathematical relationship established here between our kinetic scheme and the corresponding PBEs indicates that the former *is* the appropriate (and *microreversible*) discretization of the latter. We can exploit this fact to carry out selected simulations of the underlying kinetic model to underscore the effects of omitting/restoring microreversibility as well as to consider the effects of the presence or absence of binary cluster-cluster aggregation and other processes (e.g., inclusion or omission of irreversible grinding) in the Viedma attrition experiment.

III. CLUSTER FORMATION BY MONOMER ADDITION

The PBE models proposed for explaining the Viedma deracemization phenomena [11,12] all invoke the Gibbs-Thomson rule, which is based in turn on Gibbs thermodynamics as applied to classical nucleation theory. Since our purpose here is to establish a mathematical relationship between microreversible reaction networks [14] with those continuum population approaches, we therefore adopt the same underlying assumptions.

In classical nucleation theory [19,20], the process of formation of molecular clusters of a new phase in a background phase occurs by the addition of monomers to a spectrum of clusters of different sizes p, which are in dynamic equilibrium:

$$C_1 + C_p \underset{k_{-(p+1)}}{\overset{k_p}{\rightleftharpoons}} C_{p+1}, \quad 1 \leqslant p. \tag{3}$$

The most likely route for the formation of clusters is from a sequence of bimolecular additions [20]. This reversible kinetic scheme involves single molecules C_1, while the clusters C_p are made up from $p \geqslant 2$ molecules.

Classical nucleation theory (CNT) [14,21], in its definition of a critical size nucleus, gives estimates of the free-energy relationships for the addition/loss of monomer units to/from the growing or dissolving cluster; see Fig. 1. The solid curve represents the difference in the bulk and surface free energies of a growing cluster of p monomer units. The maximum corresponds to the critical size nucleus (critical cluster radius), which in turn corresponds to a critical number of monomer units p_{crit}, indicating the transition between endergonic to exergonic reactions. This critical size, or corresponding critical number of monomer units $p_{\text{crit}}(S)$, depends on the supersaturation value $S > 1$ and on a capillary length, which combines all the physical parameters of the particles such as surface tension, molar volume, area and volume shape factors, etc. [20].

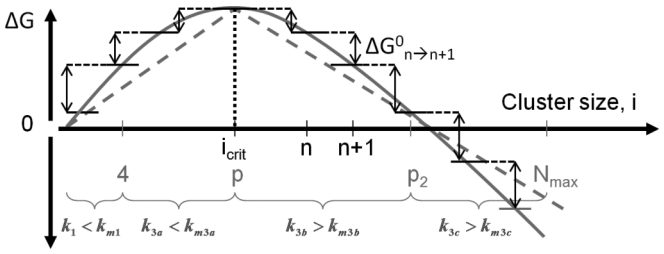

FIG. 1. Solid curve: typical profile of the Gibbs free energy of nucleation and growth by monomer addition to clusters as a function of cluster size i according to the classical nucleation theory [21] and for a given value of the supersaturation $S > 1$. The energy levels indicate the free-energy differences ΔG^0 in going from n to $n+1$ monomer units. The difference between adjacent levels $\Delta G^0_{n\to n+1}$ yields the *ratio of forward and reverse rates* at each step of monomer-to-cluster aggregation/deaggregation; see Eq. (5). The underbraces indicate a convenient isodesmic approximation employed in the simulations [14]: within each indicated cluster size subrange i, the ratio of the forward to reverse rates is a constant (compare with Fig. 4, which lists the monomer-cluster reactions for each isodesmic range).

The free-energy curve predicting the existence of a critical size nucleus shows a profile analogous to that of Fig. 1. When expressed in discrete molecular units p, this curve is given by [21]

$$\Delta G_p = -p * \Delta\mu + s_p\gamma + c, \tag{4}$$

where γ is the cluster interfacial tension, s_p is the cluster surface area, and $\Delta\mu = kT \ln S$ is the chemical potential difference in molecules transferring from solution to solid phase.

Most importantly, for equilibrium thermodynamics, the forward (attachment of a molecule) and reverse (detachment of a molecule from a cluster) rates in Eq. (3) satisfy

$$\frac{k_p}{k_{-(p+1)}} = \exp\left(\frac{-\Delta G^0_{p\to(p+1)}}{k_B T}\right), \tag{5}$$

where $\Delta G^0_{p\to(p+1)} = \Delta G^0_p - \Delta G^0_{(p+1)}$ denotes the free-energy difference between two cluster sizes that differ by a single monomer unit (see Fig. 1).

Assuming spherical clusters, then for each p there is a corresponding radius r_p; see Fig. 2. Let the mass of a molecule be δm. Then the mass of a cluster of p molecules is $m(p) = p * \delta m$. Therefore,

$$p = \frac{m(r)}{\delta m} = \frac{4\pi\rho r^3}{3\,\delta m} = \frac{4\pi r^3}{3\,\delta m/\rho} = \frac{4\pi r^3}{3\,\Omega}, \tag{6}$$

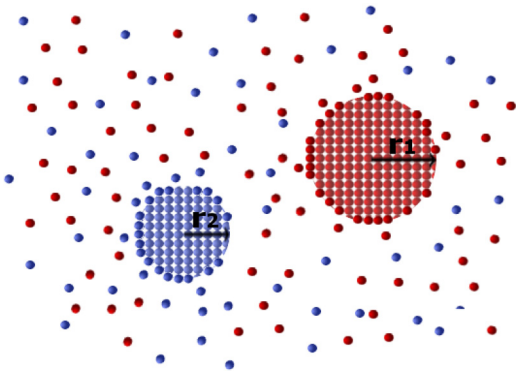

FIG. 2. (Color online) Formation of spherical chiral clusters (by monomer attachment and detachment) from the blue (dark gray) and red (light gray) enantiomers in solution. At the molecular level, both cluster growth (molecule uptake) and dissolution (detachment of molecules) are operative *simultaneously* at generally different rates; see Eq. (3). The solution phase racemization of the enantiomers can be visualized as the periodic (and rapid) interconversion of the single molecules with rate k_R.

where $\Omega = \delta m/\rho$ is the volume per molecule. The relation between radius and number of molecular units making up the spherical cluster is

$$r_p = \left(\frac{3\Omega}{4\pi}\right)^{1/3} \Rightarrow \delta r_p = r_{p+1} - r_p \sim \frac{1}{3} p^{-2/3}. \quad (7)$$

The *change* in radius δr_p depends on the cluster size p, and it goes to zero for sufficiently large p. When expressed in terms of the cluster radius, the free-energy profile Eq. (4) can be written as [20]

$$\Delta G(r) = -\left(\frac{4\pi r^3}{3\Omega}\right)\Delta\mu + (4\pi r^2)\gamma + c. \quad (8)$$

The value of the critical radius r_c follows from solving $d\Delta G(r)/dr = 0$, which yields

$$r_c = \frac{2\gamma\Omega}{\Delta\mu}, \quad (9)$$

$$\Rightarrow p_{\rm crit} = \frac{4\pi r_c^3}{3\Omega}. \quad (10)$$

IV. CONTINUUM LIMIT OF KINETIC SCHEMES

We establish a mathematical relationship between discrete microreversible kinetic schemes for cluster growth by monomer uptake from solution, Eq. (3), and the corresponding advective fluxes, Eq. (2), and growth rate functions (i.e., the $\dot{X}$) appearing in PBEs [11,12]. The continuum limit of the discrete kinetic scheme Eq. (3) leads to a population balance equation together with a mass balance equation (conservation of total system mass).

A. Becker-Döring equations

The monomer-cluster aggregation scheme Eq. (3) corresponds to the constant mass formulation of the Becker-Döring (BD) equations [22]. Consider the growth or dissolution of clusters via microreversible cluster-monomer interactions. The concentrations $\{c_p(t)\}_{p=2}^{\infty}$ satisfy

$$\frac{dc_p(t)}{dt} = J_{p-1}(t) - J_p(t) \quad (p \geqslant 2), \quad (11)$$

$$J_p(t) = k_p c_p(t) c_1(t) - k_{-(p+1)} c_{p+1}(t). \quad (12)$$

The microfluxes J_p can be positive or negative. Expanding out Eq. (11) shows that

$$\frac{dc_p(t)}{dt} = (k_{p-1}c_{p-1}(t)c_1(t) - k_{-p}c_p(t)) \quad (13)$$

$$-(k_p c_p(t) c_1(t) - k_{-(p+1)} c_{p+1}(t)), \quad (14)$$

indicating how all the forward and reverse processes contribute to the evolution of the cluster concentration $c_p(t)$. Note that the cluster growth by molecule uptake from solution and its dissolution by release of a molecule back to solution are operative *simultaneously* for all cluster sizes $p \geqslant 2$, and at generally different rates.

The monomer concentration $p = 1$ obeys the following equation:

$$\frac{dc_1(t)}{dt} = -J_1(t) - \sum_{p=1}^{\infty} J_p(t). \quad (15)$$

Then the total system mass $M(t) = \sum_{p=1}^{\infty} p\, c_p(t)$ is conserved.

B. PBE plus mass-balance equation

We now pass from an enumerable set of cluster concentrations to a single distribution function in cluster size, $c(p,t)$: that is, the density of clusters containing p-monomers at time t [23]. Then the BD and monomer evolution Eqs. (11) and (15) can be written as (note, $\Delta p = 1$ is treated as infinitesimal for large p, so that $\frac{J_{p-1}(t)-J_p(t)}{\Delta p} \to -\frac{\partial J(p,t)}{\partial p}$)

$$\frac{\partial c(p,t)}{\partial t} + \frac{\partial J(p,t)}{\partial p} = 0, \quad (16)$$

$$\frac{dc_1(t)}{dt} = -\int_0^{\infty} J(p,t)dp. \quad (17)$$

Comparison of Eq. (16) with Eq. (1) shows that this is a population balance equation for pure growth and dissolution (since $h = 0$) of clusters formed by a single species. Mass is conserved in the continuum formulation (see Appendix A). Below we derive the explicit form of the continuum advective flux $J(p,t)$ in Eq. (2) as implied by classical nucleation theory.

C. CNT and continuum advective flux

Up to this point, the above considerations are model-independent, that is, they hold for arbitrary forward and reverse reaction rates $k_p, k_{-(p+1)}$ subject only to the constraint in Eq. (5). We now appeal to classical nucleation theory (CNT) and the Gibbs-Thomson rule to model the forward and reverse rates of monomer-cluster interactions as outlined in Sec. III. See Refs. [14,20,21] for further details.

From Eqs. (4) and (5), we calculate the ratio

$$\frac{k_{-(p+1)}}{k_p} = \exp\left(\frac{\Delta G_p^o - \Delta G_{p+1}^o}{kT}\right), \tag{18}$$

$$= \exp\left(\frac{\Delta\mu - \gamma(s_{p+1} - s_p)}{kT}\right), \tag{19}$$

$$= \exp\left(\frac{\alpha}{r_p} - \frac{\gamma(s_{p+1} - s_p)}{kT}\right), \tag{20}$$

where we use $\Delta\mu = kT \ln S$ and the basic Gibbs-Thomson relationship for size-dependent solubility, $\ln S(r_p) = \frac{2\gamma\Omega}{kTr_p} = \frac{\alpha}{r_p}$ [20], and where r_p denotes the radius of a cluster containing p monomers; see Eq. (7). In other words, the existence of a critical size cluster for a given value of supersaturation S implies a size-dependent solubility $S(r_p)$ [20].

Now take the large-p limit of the flux term Eq. (12):

$$J_p(t) = k_p c_p(t) c_1(t) - k_{-(p+1)} c_{p+1}(t), \tag{21}$$

$$\cong k_p\left(c_1(t) - \frac{k_{-(p+1)}}{k_p}\right)c_p(t), \tag{22}$$

$$= k_p\left[c_1(t) - \exp\left(\frac{\alpha}{r_p} - \frac{\gamma(s_{p+1} - s_p)}{kT}\right)\right]c_p(t), \tag{23}$$

$$\Rightarrow J(p,t) = k_p\left[c_1(t) - \exp\left(\frac{\alpha}{r_p}\right)\right]c(p,t), \tag{24}$$

$$J(p,t) = G(p,t)c(p,t), \tag{25}$$

where for large p we approximate $c_p \approx c_{p+1}$, use Eq. (20), and we drop the contribution proportional to the difference in surface areas $s_{p+1} - s_p \approx 0$, as this will be negligible in this limit. We verify from the last line that $J(p,t)$ is an advective flux: compare this to Eq. (2). It is linear in the cluster distribution function $c(p,t)$, and when $G(p,t)$ is expressed in terms of cluster size (or cluster radius), it yields the empirical growth rate expressions employed in the PBEs [11] for the two-enantiomer case (see below). The advective flux Eq. (24) can be *either* positive or negative depending on whether the solute (monomer) concentration is greater or less than the size-dependent solubility, and this in turn depends on the size of the critical nucleus; see Fig. 3. The empirical growth rate $G(p,t)$ (which we have derived from microscopic considerations) can be either positive or negative:

$$G(p,t) > 0 \Leftrightarrow c_1(t) > \exp\left(\frac{\alpha}{r_p}\right), \tag{26}$$

$$G(p,t) < 0 \Leftrightarrow c_1(t) < \exp\left(\frac{\alpha}{r_p}\right), \tag{27}$$

depending on whether the (instantaneous) solute concentration is either greater than or less than the size-dependent solubility. Since a given solute concentration implies a corresponding critical size cluster, this means that the first inequality holds for cluster sizes greater than the critical size cluster, whereas the second holds for clusters smaller than the critical size cluster. In other words, the empirical growth term G implies a net growth or net dissolution for cluster sizes above or below the critical size nucleus, respectively, and for a given solute concentration (or given supersaturation). This situation is depicted graphically in Fig. 3.

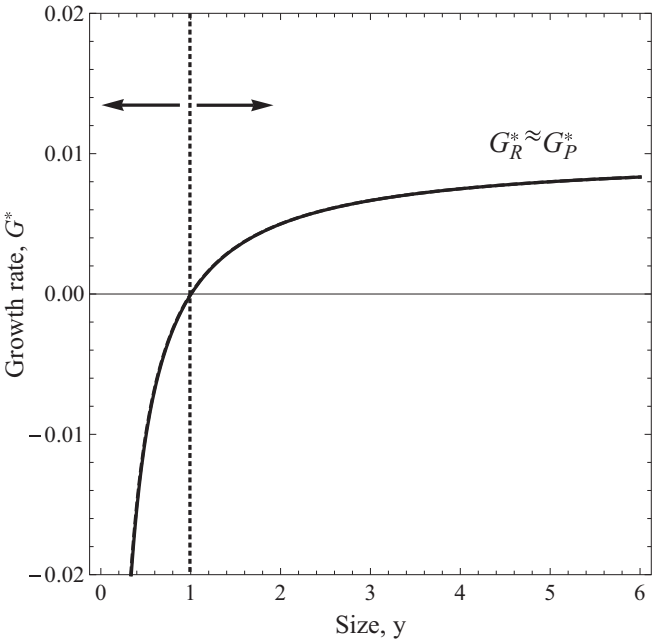

FIG. 3. Fluxes: (dimensionless) crystal growth rates $G^*_{R,P}$ vs particle size y employed in Ref. [11] for a given supersaturation $S > 1.01$ and $\alpha^* = 10^{-2}$. The arrows denote the direction of the corresponding advective fluxes $J_y = G^*(y)f(\tau,y)$: for y greater than a critical length (here equal to unity), the crystal growth rate is positive (to the right), otherwise it is negative (to the left), indicating dissolution back to monomers. But the *inverse processes* or counterfluxes, i.e., (i) precritical cluster growth up to the critical size and (ii) partial dissolution for clusters greater than the critical size, are *not* included in G^*.

This is in contrast to the microfluxes Eq. (12), which depend *simultaneously* on both molecular uptake and release of molecules and for all cluster sizes both larger and smaller than the critical nucleus: note that the microfluxes J_p and J_{p-1} individually can be either positive or negative; see Table I. The main conclusion from this section is that the continuum limit leading to the advective flux in the PBE averages out the microreversibility of the underlying kinetic scheme.

V. PBE MODEL FOR ENANTIOMERS

Below we derive a general class of population balance equations starting from our kinetic scheme [14] for growth, dissolution, solution phase racemization, binary

TABLE I. Comparison of micro- and macrofluxes. The continuum limit ($p \gg 1$) maps $J_p(t)$ to $J(p,t)$ and $[J_{p-1}(t) - J_p(t)]$ to $-\frac{\partial J(p,t)}{\partial p}$. For the macroflux, we have invoked classical nucleation theory and the Gibbs-Thomson effect.

$J_p(t)$: microflux	$J(p,t)$: macroflux
$k_p c_p(t) c_1(t) - k_{-(p+1)} c_{p+1}(t)$	$k_p(c_1(t) - \exp(\frac{\alpha}{r_p}))c(p,t)$

agglomeration, and irreversible fragmentation (attrition) for two enantiomers.

A. Growth, dissolution, and solution phase racemization

We straightforwardly generalize Eq. (3) and consider reversible growth of two chiral clusters subject to solution phase racemization of the monomers:

$$L_1 + L_p \underset{k_{-(p+1)}}{\overset{k_p}{\rightleftharpoons}} L_{p+1}, \quad D_1 + D_p \underset{k_{-(p+1)}}{\overset{k_p}{\rightleftharpoons}} D_{p+1}, \tag{28}$$

$$L_1 \underset{k_R}{\overset{k_R}{\rightleftharpoons}} D_1. \tag{29}$$

Then the continuum limit of this kinetic reaction scheme is immediate from Secs. IV B and IV C:

$$\frac{\partial c_i(p,t)}{\partial t} + \frac{\partial J_i(p,t)}{\partial p} = 0 \quad (i = L,D), \tag{30}$$

$$\frac{dc_L(t)}{dt} = -\int_0^\infty J_L(p,t)dp + k_R(c_D - c_L), \tag{31}$$

$$\frac{dc_D(t)}{dt} = -\int_0^\infty J_D(p,t)dp + k_R(c_L - c_D), \tag{32}$$

where $c_L, c_D = [L_1],[D_1]$, $c_j(p,t)$ denotes the distribution function of clusters of handedness $j = L,D$, and where the advective fluxes and growth rates are

$$J_i(p,t) = G_i(p,t)c_i(p,t), \tag{33}$$

$$G_i(p,t) = k_p(c_i(t) - \exp(\alpha/r_p)). \tag{34}$$

The total system mass $c_L(t) + c_D(t) + \int_0^\infty p[c_L(p,t) + c_D(p,t)]dp$ is conserved (see Appendix A).

B. Reversible binary agglomeration

The above considerations have dealt with pure growth and dissolution processes. To complete the picture, we turn to *reversible* cluster-cluster aggregation and then finally irreversible binary fragmentation (i.e., mechanical grinding). The kinetics of the former process can be represented as follows, and for a single chemical species,

$$C_p + C_s \underset{b_{p,s}}{\overset{a_{p,s}}{\rightleftharpoons}} C_{p+s}, \tag{35}$$

where the aggregation rate coefficients $a_{p,s}$ are referred to collectively as the aggregation kernel. The rates for the *inverse* aggregation process $b_{p,s}$ are denoted collectively as the fragmentation or deaggregation kernel.

From the law of mass-action, Smoluchowski wrote down the differential equations for binary cluster aggregation and fragmentation [22,24]:

$$\frac{dc_p(t)}{dt} = \frac{1}{2}\sum_{s=1}^{p-1} J_{s,p-s} - \sum_{s=1}^{\infty} J_{p,s}, \tag{36}$$

where the aggregation fluxes are given by

$$J_{p,s} = a_{p,s}c_p c_s - b_{p,s}c_{p+s}, \tag{37}$$

$$J_{s,p-s} = a_{s,p-s}c_s c_{p-s} - b_{s,p-s}c_p. \tag{38}$$

We now take the continuum limit of Eq. (36) to arrive at

$$\begin{aligned}\frac{\partial c(p,t)}{\partial t} = {} & \frac{1}{2}\int_0^p a(s,p-s)c(s,t)c(p-s,t)ds \\ & - c(p,t)\int_0^\infty a(p,s)c(s,t)ds \\ & - \frac{1}{2}c(p,t)\int_0^p b(s,p-s)ds \\ & + \int_p^\infty b(p,s-p)c(s,t)ds. \end{aligned} \tag{39}$$

The first two terms correspond to source and sink terms arising from a binary aggregation process, see Sec. 3.3.5 in Ref. [15]. The latter two terms correspond to *reverse aggregation* or binary fragmentation. The above equation is expressed in terms of the cluster mass [recall, the cluster mass $m(p) = \delta m * p$ is proportional to the number of molecular units]. When expressed in terms of cluster size (see Chap. 6 of Ref. [17]), the first two contributions yield the same mathematical structure (integrals, limits, and kernels) as the explicit agglomeration terms employed in population balance modeling [11], provided we identify $a_{p,s}$ with the specific continuum kernels employed there. In this way, we also verify that the latter two terms in Eq. (39) are *absent* from those specific population models [11,12].

Thus, incorporating such an irreversible process in the h term, Eq. (1), constitutes an assumption of kinetic control in the binary agglomeration process and reduces the scope of the thermodynamic description of the process. Notice that mechanical grinding is not the *inverse* of agglomeration, and this is taken up in the following section.

C. Irreversible binary fragmentation

The *mechanical grinding* of clusters into two fragments can be represented as follows, and for a single chemical species:

$$C_{p+s} \overset{f_{p,s}}{\rightarrow} C_p + C_s. \tag{40}$$

We remark that irreversible fragmentation is what prevents the system from being able to reach the conditions leading to thermodynamic equilibrium. In the continuum language, this gives the fragmentation contributions appearing in the PBE models [11,12] provided we identify $f_{p,s}$ with the specific continuum kernels employed there. From the previous considerations, we can immediately write down the contribution of binary fragmentation to the evolution of populations of clusters, namely,

$$\begin{aligned}\frac{\partial c(p,t)}{\partial t} = {} & \int_p^\infty f(p,s-p)c(s,t)ds \\ & - \frac{1}{2}c(p,t)\int_0^p f(s,p-s)ds, \end{aligned} \tag{41}$$

$$= 2\int_p^\infty b(u)P(p|u)c(u,t)du - b(p)c(p,t). \tag{42}$$

The relation between Smoluchowski's fragmentation kernels $f_{p,s}$ and the breakage functions commonly employed in

population balance modeling is given as follows:

$$f(p,s-p) = \nu(s)b(s)P(p|s), \tag{43}$$

$$f(s,p-s) = \nu(p)b(p)P(s|p), \tag{44}$$

where $\nu(x)$ is the average number of particles formed from the breakup of a single particle of mass x [$\nu(x) = 2$ for binary breakup], $b(x)$ is the fraction of particles of mass x breaking per unit time, and $P(x|x')$ is the probability density for particles from a breakup of mass x' to have mass x, and it obeys the constraint $\int_0^{x'} P(x|x')dx = 1$ [15].

The full PBE including growth, dissolution, (reversible) agglomeration, and mechanical grinding is obtained by substituting $c(p,t) \to c_i(p,t)$ for $i = L,D$ on the right-hand sides of Eqs. (39) and (42) and then adding these terms to the right-hand side of Eq. (30). This completes the demonstration that the continuum limit of the kinetic scheme [14] leads to population balance equations of the form presented above in Eq. (1), including the h terms, and with the explicit advective flux for growth, Eq. (2), derived from first principles (classical nucleation theory and the Gibbs-Thomson effect).

Apart from the reversible agglomeration, this establishes the relationship between the general kinetic scheme in [14] and the class of population balance models [11,12]: the latter arise from taking the continuum limit of the former.

VI. RESULTS: SIMULATIONS

Our main results above demonstrate that the kinetic reaction scheme in Eqs. (28), (29), (35), and (40) can be regarded as a bona-fide discretization of the continuum population balance equations to which it gives rise. Numerical simulations of this kinetic scheme indicate that the Viedma deracemization phenomenon corresponds to a true SMSB scenario [14], and that this scheme meets the challenge of being capable of absolute asymmetric synthesis (AAS). Below we use this kinetic scheme to simulate the PBEs [25], providing a few illustrative examples in order to highlight the effects of reversible versus irreversible transformations on pure growth and dissolution (recall the discussion in Sec. IV C), kinetic versus thermodynamic control, the role of (reversible) agglomeration, as well as the effects of irreversible mechanical grinding.

Full details of the complete kinetic network parameters, rate constants, isodesmic approximations used for the free-energy profile, and the sizes of clusters involved in both the aggregation and in the fragmentation processes have been published previously, as has an in-depth discussion of the numerical methodology employed [14]. However, we make special mention of the initial conditions employed in all the simulations below. Unless otherwise stated, these are as follows: (a) $[D]_0 = [L]_0 = 0.5\ \mathrm{mol}\,l^{-1}$, $[D_{N\max}]_0 = 6\ \mathrm{mol}\,l^{-1}$, $[L_{N\max}]_0 = (6 + 1 \times 10^{-13})\ \mathrm{mol}\,l^{-1}$, and the initial concentrations of the rest of the species (all the intermediate sized clusters) were set equal to zero, or (b) $[D]_0 = [L]_0 = 0.5\ \mathrm{mol}\,l^{-1}$, $[D_{N\max}]_0 = 4\ \mathrm{mol}\,l^{-1}$, $[L_{N\max}]_0 = 8\ \mathrm{mol}\,l^{-1}$, and the initial concentrations of the rest of the species were set equal to zero; in all cases, $N_{\max} = 70$. The former corresponds to starting the system off from a very small initial ee, smaller than that expected for a statistical fluctuation about the ideal racemic composition: ee% $= (1 \times 10^{-12})$% [2]. We do so in order to see if the scheme is capable of AAS. The latter conditions represent a much larger initial ee, of roughly 33%.

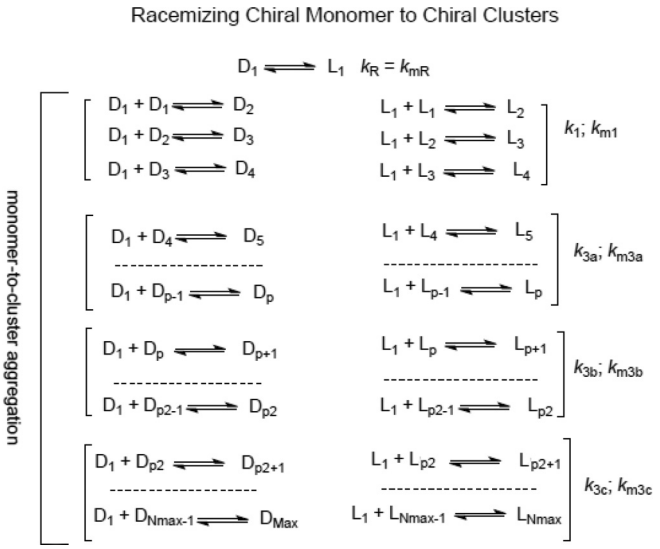

FIG. 4. Scheme 1: kinetic scheme based on the free energy diagram for classical theory of primary nucleation. A racemizing monomer pair (L_1, D_1) in solution (rate $k_R = k_{mR}$) and monomer-cluster aggregation yielding chiral aggregates of a maximum size $(L_{N\max}, D_{N\max})$. The network approximates the free energy curve in Fig. 1 by four isodesmic regions (indicated by the reaction steps grouped within the vertical brackets), whose end points are (i) a precritical cluster size we fix to be four monomer units, (ii) the critical cluster size denoted $p = i_{\mathrm{crit}}$, (iii) a postcritical cluster of $p_2 > p$ units, and (iv) chiral clusters of maximum size $N_{\max}$. $(2 \to 4)$: rates k_1, k_{m1}; $(4 \to p)$: rates k_{3a}, k_{m3a}; $(p \to p_2)$: rates k_{3b}, k_{m3b}; and $(p_2 \to N_{\max})$: rates k_{3c}, k_{m3c}.

A. Pure growth and dissolution

We first consider pure growth and dissolution processes by means of our kinetic scheme (Fig. 4), simulating a virtual case of a constant supersaturation value $S > 1$, i.e., when the free-energy curve in Fig. 1 remains constant in time, and comparing the outcome first for irreversible and then for reversible rates. If we use either of the initial conditions (a) or (b) summarized above, no amplification is detected (data not shown) in either case, not even starting from a rather large initial ee.

On the other hand, if we adopt initial chiral cluster concentrations given by Gaussian distributions, and in order to mimic those employed in Ref. [11], then very different outcomes are observed. The difference is, we start the system off with an initial spectrum of cluster sizes centered about a mean value. To proceed, we take each chiral family of initial clusters to be centered at *different* mean values (p, p_2); we take equal initial widths $\sigma_L = 1, \sigma_D = 1$, and set $a = 5$. The initial concentrations for clusters comprised of n-monomer units are described as follows:

$$L_n(0) = \frac{a}{n}\exp[-(n-p)^2/\sigma_L], \tag{45}$$

$$D_n(0) = \frac{a}{n}\exp[-(n-p_2)^2/\sigma_D]. \tag{46}$$

These imply equal initial masses for each population of enantiomers: $\sum nL_n(0) = \sum nD_n(0)$. The time-dependent enantiomeric excesses we calculate are given by

$$\mathrm{ee}_n(\%) = (L_n - D_n)/(L_n + D_n) \times 100, \tag{47}$$

$$\mathrm{ee}(\%) = \sum_{n=2}^{N_{\max}} [n(L_n - D_n)] \Big/ \sum_{n=2}^{N_{\max}} [n(L_n + D_n)] \times 100. \tag{48}$$

The former depends on the individual cluster size $2 \leqslant n \leqslant N_{\max}$ and the latter gives a measure of net mass-averaged chiral excess, and it corresponds to the enantiomeric excess measure used in Ref. [11]. The measure in Ref. [11] includes all cluster sizes down to the monomer, whereas our measure starts off with the dimer.

Kinetic control: Irreversible rates were enforced by dropping the *forward* rates of precritical cluster growth $k_1 = k_{3a} = 0$ from $i = 2$ up to $p = i_{\mathrm{crit}}$ as well as dropping the rates for postcritical cluster deaggregation (dissolution) for clusters of sizes $i > i_{\mathrm{crit}}$, back down to i_{crit}: thus we set $k_{m3b} = k_{m3c} = 0$ for all sizes $n > i_{\mathrm{crit}}$ greater than the critical size; see Fig. 1. This setting of these null rate constants mimics the strict dissolution or strict growth of clusters below or above the critical-sized cluster, respectively, and it is the very feature enforced by the continuum growth functions $G(p,t)$ appearing in the population balance models (see also Fig. 3).

For our simulations, we take $N_{\max} = 70$, $p = 10$, $p_2 = 30$ and the reaction rates $k_{m1} = 4 \times 10^4$, $k_{m3a} = 150$, $k_{3b} = 100$, $k_{3c} = 100$ and the solution phase racemization rate $k_R = 10^6$. The overall system ee(%) decreases from its small initial value to about -40% and remains locked in at this value for the remainder of the simulation times; see Fig. 5 (top). Since the initial distribution of the L_n clusters is smaller than that of the D_n clusters, the former dissolve preferentially (the Gibbs-Thomson effect), and via solution phase racemization, they contribute to the growth of the D_n clusters: hence the final ee is negative. Figure 5 (bottom) displays the gradient in ee_n indicating how the initial individual ee_n's evolve in time. The ee of each cluster depends on its size, as measured in monomer units. The set of ee_n's shows a complex behavior, reflecting the spread in the initial $\mathrm{ee}_n(0)$ coming from the Gaussians (the "*sufficiently different initial sizes*") [11]. For times $t(s) \gg 0.1$, a gradient pattern sets in indicating how each cluster size is locked in (kinetically) to a specific chiral excess.

Thermodynamic control: In marked contrast, when microreversibility is reinstated, $k_1 = 10^4$, $k_{3a} = 10^2$, $k_{m3b} = 90$, $k_{m3c} = 90$ (Fig. 6). Then for the remaining rates and initial conditions as before, the system undergoes a short duration *chiral excursion* before ending up in the inevitable final racemic state: the earliest stages of the reaction network come under kinetic control, but the late-time asymptotic regime comes under thermodynamic control. Note how the mass-averaged ee resolves into the complex pattern of the individual ee_n for each cluster size; see the bottom of Fig. 6. Despite the initially wide spectrum of enantiomeric excesses, these all converge to zero under thermodynamic control. Very small but nonzero values for these rate constants merely postpone the inevitable approach to the asymptotic racemic

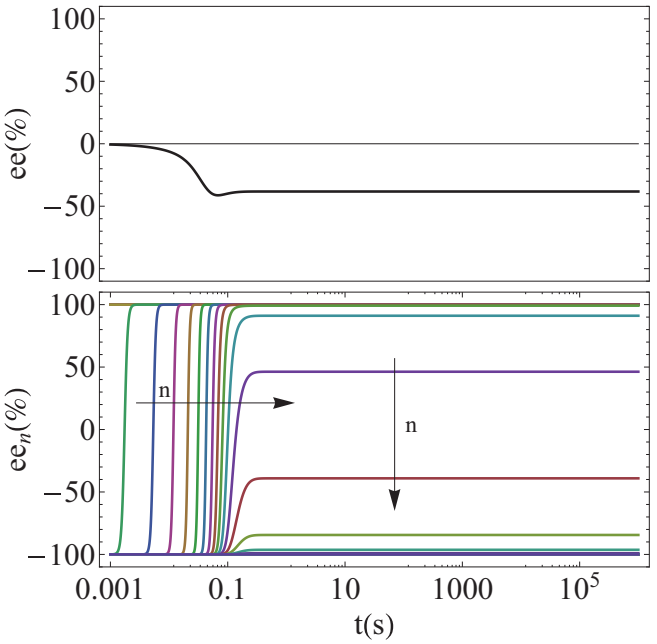

FIG. 5. (Color online) Kinetic control: simulation showing the effect of using *irreversible* rates (i.e., setting $k_1 = k_{3a} = k_{m3b} = k_{m3c} = 0$ in Fig. 4). That is, we shut off growth of precritical clusters up to the critical size and degradation of postcritical clusters back down to the critical size. Bottom: the enantiomeric excesses $\mathrm{ee}_n(\%)$ for clusters of size $2 \leqslant n \leqslant N_{\max}$. The gradient from small to large n is indicated by the arrows.

state. The only difference between this and the former outcome is that here we allow for cluster growth up to the critical size cluster and also dissolution of clusters greater than the critical size cluster: all transformations involved are fully reversible.

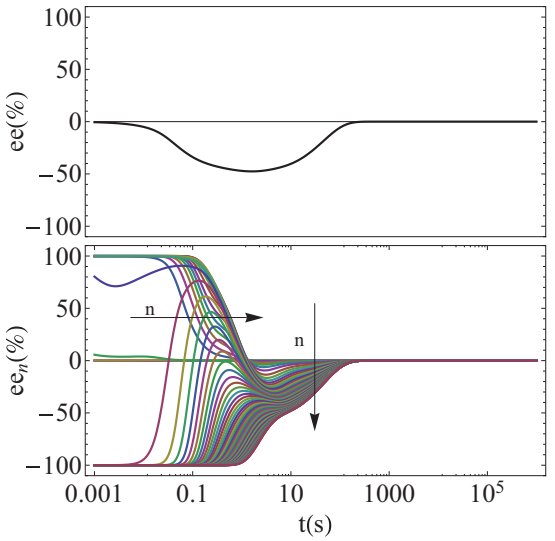

FIG. 6. (Color online) Thermodynamic control: simulation showing the effect of using fully reversible rates, i.e., for $k_1 = 10^4$, $k_{3a} = 10^2$, $k_{m3b} = 90$, $k_{m3c} = 90$ in Fig. 4. Bottom: enantiomeric excesses $\mathrm{ee}_n(\%)$ for clusters of size $2 \leqslant n \leqslant N_{\max}$. The gradient from small to large n is indicated by the arrows. Compare with Fig. 5.

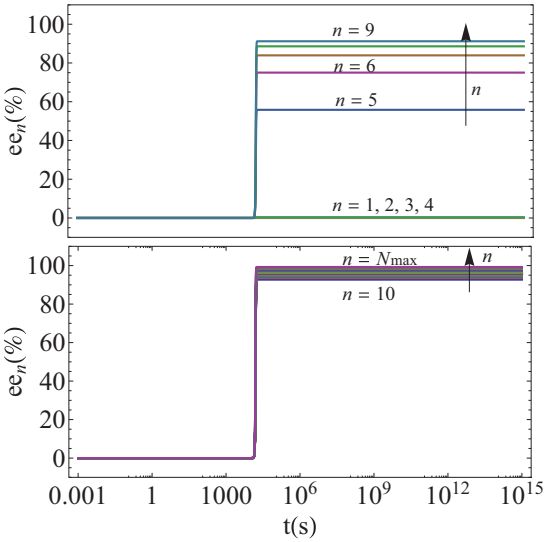

FIG. 7. (Color online) Full kinetic model [14] with reversible agglomeration. Initial conditions: tiny initial ee: ee% $= 1 \times 10^{-12}$%, type (a) (see text). This provides a striking example of absolute asymmetric synthesis.

B. Presence or absence of reversible agglomeration

A characteristic and illustrative example of the different final states achieved in the presence or in the absence of cluster-to-cluster agglomeration is shown in Figs. 7 and 8, respectively. In the presence of cluster-to-cluster agglomeration, a final chiral state is obtained, but in its absence, and even when starting from a significant initial ee, the final outcome is a racemic stationary state: after an initial chirality transfer to the rest of clusters, the system cannot retain the initial ee and eventually racemizes (permanent mirror symmetry is recovered); see Fig. 8.

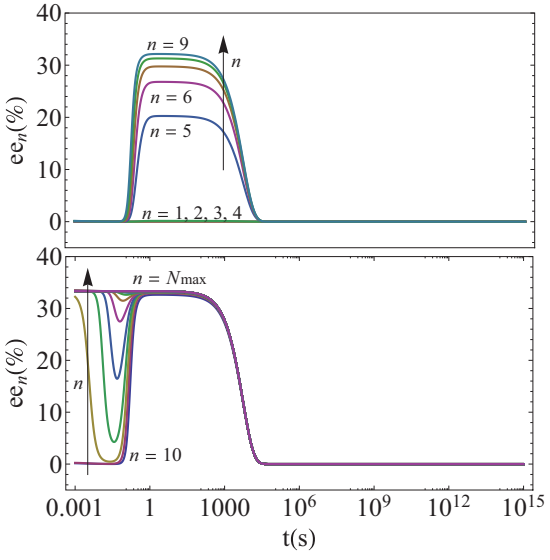

FIG. 8. (Color online) Full kinetic model [14] without agglomeration. Initial conditions are large, ee = 33%: type (b) (see text). Kinetic controlled temporary chiral amplification (chiral excursion).

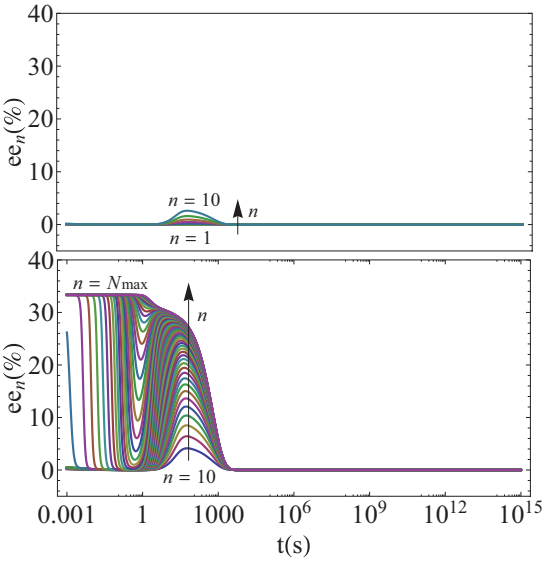

FIG. 9. (Color online) Full model without grinding: Initial conditions are large, ee = 33%: type (b) (see text). Short-lived chiral amplification followed by the final racemic state.

Note that a recent report [12] using PBE's claimed to achieve chiral amplification without agglomeration. A careful consideration of the unorthodox "growth" term employed by those authors reveals, however, that it actually corresponds to an agglomeration characterized by a singular agglomeration kernel (for the proof of this, see Appendix B).

C. No grinding

In contrast to Fig. 7, which shows reversible agglomeration in the presence of grinding, we consider agglomeration without grinding. Even when starting from large initial ee, and for the same rates used in the simulation leading to Fig. 7, the system eventually racemizes; see Fig. 9. This underscores the importance of grinding, which, on the basis of the approximation leading to net flows in PBEs, has been claimed to be unnecessary for obtaining a final chiral state in a closed system with a homogeneous temperature distribution (e.g., see the second paper in Ref. [11]).

Most importantly, the simulations demonstrate that (i) in the absence of agglomeration but even with irreversible grinding, the final outcome will be racemic (Fig. 8); (ii) with agglomeration operative but no grinding, the outcome will be racemic (Fig. 9). Only for the case (iii) when both agglomeration and irreversible grinding are operative simultaneously can the system lead to a final chiral outcome, and with large enantiomeric excesses close to 100% for the largest chiral clusters (Fig. 7).

Recall that absolute asymmetric synthesis (AAS) is the transformation of achiral or racemizing products in the absence of any chiral polarization (i.e., circularly polarized light, hydrodynamic vortices, chiral contaminants, etc.) to chiral products in detectable enantiomeric excess levels [3]. AAS may occur in networks leading to a bifurcation scenario with subsequent amplification of the initial chiral fluctuations about the ideal racemic (mirror symmetric) composition. Since

for AAS there is no chiral bias, one expects a stochastic distribution of signs (plus/minus) in the final enantiomeric excesses between successive experiments, precisely because the sign of the initial chiral fluctuation is random (there is no bias). This in turn must lead to a *bimodal distribution* in the signs of the final chiral outcomes (as well as for temporary chiral amplifications ending up as racemic final states). To test this ability of our kinetic scheme, we repeat the simulations reported above in Figs. 7–9, now flipping the sign of the initial enantiomeric excesses. The series of results [27] demonstrate that the final enantiomeric excesses also change sign as well, that is, they follow the sign of the initial chiral perturbation. Hence, a random distribution of initial chiral perturbations will lead to a bimodal distribution in final chiral outcomes, the essential hallmark of AAS. This is in accord with the observed experimental results; see the first paper in Ref. [8].

VII. DISCUSSION AND CONCLUSIONS

The *continuum limit* of a kinetic reaction scheme involving growth, dissolution, solution-phase racemization, binary agglomeration, and mechanical fragmentation [14] yields the general class of population balance equations (PBEs) that have been used recently in attempts to model the Viedma deracemization phenomenon [11,12]. This result in and of itself constitutes the main result of this paper. Among other things, it establishes a mathematical connection between chemical kinetic schemes and continuum population balance modeling, demonstrating that both approaches are really two complementary sides of the same coin. The continuum limit reveals moreover that even if one accounts for detailed balance (microreversibility) at the kinetic level, it is lost in the growth and dissolution rate functions appearing in the PBEs. This means that those functions are a source of kinetic control (since they represent irreversible processes). Moreover, we have also verified that the aggregation or agglomeration terms employed in those particular PBE models do not account for the *inverse* processes of deagglomeration (binary fragmentation) and thus contribute a further source of kinetic control.

These findings are of capital importance if one wishes to use PBEs to study spontaneous mirror symmetry breaking (SMSB) or absolute asymmetric synthesis. Here we use SMSB as a synonym of thermodynamically controlled absolute asymmetric synthesis, i.e., as a transformation where the racemic state is metastable and a degenerate chiral state (scalemic mixture as final outcome) is the final (long-time) stable state of the system. This can only occur under experimental conditions preventing the evolution of the system (open or closed) toward thermodynamic equilibrium. The chemical significance of the phenomenon of SMSB is that it takes place under microreversible constraints within the framework of linear thermodynamics of irreversible processes. The thermodynamic rationalization of such spontaneous mirror symmetry breaking is the achievement of an asymptotic stable chiral state that, in the framework of irreversible thermodynamics, is characterized by minimum entropy production [6]. Nevertheless, in closed systems that come into thermodynamic equilibrium with their surroundings, *kinetically controlled* absolute asymmetric synthesis is possible: a *temporary* amplification of chirality results that may be useful in applied synthesis [4]. These considerations do not invalidate or question the use of PBMs in common crystallizations, implying a supersaturation value that decreases in time accompanied by a fast secondary nucleation process, nor the description they give of preferential crystallizations. Indeed, such population balance modeling is intended to simulate a kinetically controlled crystallization process [28,29].

The kinetic and population balance models treated here are based on the mean-field approximation, so it may be worthwhile to mention some basic statistical mechanical and stochastic properties of the chiral phase transition in chemical systems. For technical reasons, the study of statistical mechanical aspects of chiral symmetry breaking in chemical systems is best investigated using simpler reaction schemes based, for example, on Frank's original model. The Frank model captures the essence of chiral symmetry breaking but falls short of being able to explain more involved phenomena such as Viedma deracemization [14]. Having said this, we summarize some of the pertinent results as follows:

A useful statistical approach to chiral symmetry breaking starts from the chemical master equation for birth-death processes on a spatial lattice, providing an exact description of the Frank model dynamics on the microscopic level [30]. This solution can be cast in terms of a quasi-Schrödinger equation with an associated non-Hermitian "Hamiltonian." Simulations of Langevin equations derived from this master equation approach indicate that the growth of chiral domains from initially spatially extended racemic configurations (in a two-dimensional reaction domain) grow by front propagation until the entire available computation domain is occupied by a single chirality. Sometimes the end-result consists of two subdomains of opposite chirality within a single computational domain, representing a stable outcome with a global net zero ee. In such a statistical treatment, long-range chiral correlations (bounded above by the system's finite size) emerge from the local autocatalytic growth of the enantiomers of the same handedness, and once one homochiral domain "wins" territory, it persists stably as long as the system is maintained out of equilibrium.

In a related vein, dynamic critical properties of a simple variant of the Frank model demonstrate that the dynamic phase transitions of the latter are in the same *universality class* as statistical models of directed percolation [31]. The inherent stochasticity arises from the internal reaction noise (as typified by the chemical master equation approach).

The effective potential can be calculated for the Frank model in which external noise is introduced to account for random environmental effects [32]. The well-mixed limit, corresponding to negligible diffusion and also finite diffusion in two spatial dimensions, is considered. White noise has a disordering effect, whereas in the latter two-dimensional case, a true chiral phase transition occurs for external noise exceeding a critical intensity which racemizes the system, that is, a sufficiently strong external noise *restores* the chiral symmetry.

Finally, the fundamental interest of any model/approach regarding the question of the origin of biological homochirality lies in its ability for absolute asymmetric synthesis and the amplification of the tiny statistical chiral fluctuations about

the ideal racemic composition up to observable ee levels [2]. The required "*sufficient difference between the initial particle size distributions*" postulated in the mechanism in Ref. [11] does not satisfy this necessary precondition to be of interest for speculations concerning the origin of biological homochirality. Such a condition could only lead to a deterministic selection of one of the two chiral signs, but it is not at all a condition for the *emergence* of chirality as a steady final state. The nature of thermodynamic control implies, moreover, that for the same system parameters and total chemical mass, the final state must be the same independent of the initial relative concentrations of the species involved in the transformations. An understanding of how biological homochirality might have arisen begins with the study of reaction networks leading to chiral states within the framework of nonequilibrium microreversible chemical transformations.

ACKNOWLEDGMENTS

We acknowledge useful correspondence with Doraiswami Ramkrishna (College of Engineering, Purdue University). This research was supported in part by Grant No. CTQ2013-47401-C2-1/2-P (MINECO) and forms part of the COST Action CM1304 on "Systems Chemistry" (J.M.R. and D.H.)

APPENDIX A: MASS CONSERVATION

Define $M(t) = \int_0^\infty p\, c(p,t)dp$. Then $M(t) + c_1(t)$ is conserved:

$$\frac{dM(t)}{dt} = \int_0^\infty p \frac{\partial c(p,t)}{\partial t} dp, \tag{A1}$$

$$= -\int_0^\infty p \frac{\partial J(p,t)}{\partial p} dp, \tag{A2}$$

$$= [-pJ(p,t)]_{p=0}^{p\to\infty} + \int_0^\infty J(p,t)dp \tag{A3}$$

$$= \int_0^\infty J(p,t)dp, \tag{A4}$$

$$= -\frac{dc_1(t)}{dt}, \tag{A5}$$

using Eqs. (16) and (17) and the boundary conditions that particle distributions vanish at zero, $c(0,t) = 0$, and at infinity, $\lim_{p\to\infty} c(p,t) = 0$ [15]. The generalization to the two-enantiomer case in Sec. V is immediate; the corresponding boundary conditions are $c_i(0,t) = 0$ and $\lim_{p\to\infty} c_i(p,t) = 0$ for $i = L, D$.

APPENDIX B: CRYPTO-AGGLOMERATION AND THREE-BODY INTERACTIONS

Here we prove that the unusual growth rate ($i = L, D$)

$$G_{i,R} = k'(1 + \Gamma_{i,R})\big(C_{i,0} - C_R^{\rm sol}\big), \tag{B1}$$

$$= k'[1 + k'' f_i(R,t)R^2]\big(C_{i,0} - C_R^{\rm sol}\big), \tag{B2}$$

$$= k'\big(C_{i,0} - C_R^{\rm sol}\big) + k'k'' f_i(R,t)R^2\big(C_{i,0} - C_R^{\rm sol}\big), \tag{B3}$$

proposed in Ref. [12], corresponds to an agglomeration, albeit a singular one (to facilitate the demonstration, we employ the same notation). When multiplied by the particle distribution, it yields a *second-order term* $\sim k'k'' f_i^2$ in the particle distribution function f_i. Comparison with the *general* PBE Eqs. (1) and (2) shows that this contribution corresponds to neither an advective nor a diffusive *flux* [15]. Only these two types of fluxes are allowed in the general PBE framework. This term, however, can be expressed either as (i) a two-cluster agglomeration integral with a singular kernel or (ii) as a three-body reaction involving two clusters and a molecule. This second alternative (ii) is rather unlikely to occur in ordinary solution chemistry unless either very high concentrations are achieved or the reactions take place in viscous media. Neither is the case for the Viedma deracemization experiment.

Agglomeration in a PBE framework generally yields both birth and death terms [15]. We consider here just the death term (meaning that particles of radius R are depleted from the overall population):

$$Q_i(R) = \int_0^\infty \beta_i(R,\lambda) f_i(\lambda,t) f_i(R,t) d\lambda, \tag{B4}$$

with the singular agglomeration kernel β:

$$\beta_i(R,\lambda) = k'k''\lambda^2\big(C_{i,0} - C_\lambda^{\rm sol}\big)\frac{d}{d\lambda}\delta(\lambda - R). \tag{B5}$$

Calculate the rate of disappearance of particles of radius R from the overall population:

$$Q_i(R) = \int_0^\infty \beta_i(R,\lambda) f_i(\lambda,t) f_i(R,t) d\lambda$$

$$= \int_0^\infty k'k''\lambda^2\big(C_{i,0} - C_\lambda^{\rm sol}\big)\frac{d}{d\lambda}\delta(\lambda - R) \times f_i(\lambda,t) f_i(R,t) d\lambda, \tag{B6}$$

$$= \lim\Big[k'k''\lambda^2\big(C_{i,0} - C_\lambda^{\rm sol}\big) \times f_i(\lambda,t) f_i(R,t)\delta(\lambda - R)\Big]_{\lambda\to 0}^{\lambda\to\infty} - \frac{\partial}{\partial R}k'k''R^2\big(C_{i,0} - C_R^{\rm sol}\big) f_i(R,t) f_i(R,t), \tag{B7}$$

$$= -\frac{\partial}{\partial R}k'k''R^2\big(C_{i,0} - C_R^{\rm sol}\big) f_i(R,t) f_i(R,t). \tag{B8}$$

We verify that (B8) corresponds identically to Eqs. (6) and (9) in Ref. [12]. This proves that the $k'k''$ contribution to the "growth term" (B3) represents an agglomeration process [or *crypto-agglomeration*, since it is concealed or camouflaged by an unorthodox growth rate expression (B3)].

From inspection, we see that the product $G_{i,R} f_i(R,t)$ represents a *three-body* interaction (monomer-cluster-cluster) since it contains the contribution $C_{i,0} f_i(R,t) f_i(R,t)$.

[1] D. Kondepudi and G. Nelson, Phys. A **125**, 465 (1984); D. K. Kondepudi, I. Prigogine, and G. Nelson, Phys. Lett. A **111**, 29 (1985); V. A. Avetisov, V. V. Kuz'min, and S. A. Aniki, Chem. Phys. **112**, 179 (1987); D. K. Kondepudi, BioSystems **20**, 75 (1987); V. Avetisov and V. Goldanskii, Proc. Natl. Acad. Sci. USA **93**, 11435 (1996).

[2] W. H. Mills, Chem. Ind. (London) **51**, 750 (1932); V. I. Goldanskii and V. V. Kuzmin, Z. Phys. Chem. **269**, 216 (1988); K. Mislow, Collect. Czech. Chem. Commun. **68**, 849 (2003).

[3] J. M. Ribó, C. Blanco, J. Crusats, Z. El-Hachemi, D. Hochberg, and A. Moyano, Chem. Eur. J. **20**, 17250 (2014).

[4] J. Crusats, D. Hochberg, A. Moyano, and J. M. Ribó, ChemPhysChem **10**, 2123 (2009).

[5] K. Soai, T. Shibata, H. Morioka, and K. Choji, Nature (London) **378**, 767 (1995); K. Soai and T. Kawasaki, in *Asymmetric Synthesis—The Essentials*, edited by M. Christmann and S. Brse (Wiley-VCH, Weinheim, 2007), pp. 212–216; T. Kawasaki, Y. Matsumura, T. Tsusumi, K. Suzuki, M. Ito, and K. Soai, Science **324**, 492 (2009); A. Matsumoto, S. Oji, S. Takano, K. Tada, T. Kawasaki, and K. Soai, Org. Biomol. Chem. **11**, 2928 (2013).

[6] D. Kondepudi and I. Prigogine, *Modern Thermodynamics* (Wiley, Chichester, 1999), pp. 392–402.

[7] For a description of crystal racemic conglomerates and of the compounds able to yield them, see J. Jacques, A. Collet, and S. H. Wilen, *Enantiomers, Racemates and Resolutions* (Wiley, New York, 1981), pp. 35 and 36.

[8] C. Viedma, Phys. Rev. Lett. **94**, 065504 (2005); Cryst. Growth Des. **7**, 553 (2007); W. L. Noorduin, T. Izumi, A. Millemaggi, M. Leeman, H. Meekens, W. J. P. van Enckevort, R. M. Kellogg, B. Kaptein, E. Vlieg, and D. G. Blackmond, J. Am. Chem. Soc. **130**, 1158 (2008); W. L. Noorduin, H. Meekes, W. J. P. van Enckevort, A. Millemaggi, M. Leeman, B. Kaptein, R. M. Kellog, and E. Vlieg, Angew. Chem. **120**, 6545 (2008); Angew. Chem. Int. Ed. **47**, 6445 (2008); B. Kaptein, W. L. Noorduin, H. Meekes, W. J. P. van Enckvort, R. M. Kellogg, and E. Vlieg, Angew. Chem. **120**, 7336 (2008); Angew. Chem. Int. Ed. **47**, 7226 (2008); C. Viedma, J. E. Ortiz, T. de Torres, T. Izumi, and D. G. Blackmond, J. Am. Chem. Soc. **130**, 15274 (2008); W. K. Rybak, Tetrahedron: Asymmetry **19**, 2234 (2008); S. B. Tsogoeva, S. Wei, and M. Mauksch, Angew. Chem. **121**, 598 (2009); Angew. Chem. Int. Ed. **48**, 590 (2009); M. P. S. Cheung, M. S. Pui, and L. A. Cuccia, Chem. Commun. **45**, 1337 (2009); G. Levilain, C. Rougeot, F. Guillen, J.-C. Plaquevent, and G. Cocquerel, Tetrahedron: Asymmetry **20**, 2769 (2009); W. L. Noorduin, P. van der Asdonk, H. Meekes, W. J. P. van Enckervort, B. Kaptein, M. Leeman, R. M. Kellogg, and E. Vlieg, Angew. Chem. **121**, 3328 (2009); Angew. Chem. Int. Ed. **48**, 3278 (2009); S. Wei, M. Mauksch, and S. B. Tsogoeva, Chem. Eur. J. **15**, 10255 (2009); A. Flock, C. M. M. Reucher, and C. Bolm, *ibid.* **16**, 3918 (2010); W. L. Noorduin, H. Meekes, W. J. P. van Enckevort, B. Kaptein, R. M. Kellogg, and E. Vlieg, Angew. Chem. **122**, 2593 (2010); Angew. Chem. Int. Ed. **49**, 2539 (2010).

[9] M. Uwaha, J. Phys. Soc. Jpn. **73**, 2601 (2004); J. Crusats, S. Veintemillas-Verdaguer, and J. M. Ribó, Chem. Eur. J. **12**, 7776 (2006); C. Viedma, Astrobiology **7**, 312 (2007); D. G. Blackmond, Chem. Eur. J. **13**, 3290 (2007); J. H. E. Cartwright, O. Piro, and I. Tuval, Phys. Rev. Lett. **98**, 165501 (2007); L. W. Noorduin, H. Meekes, A. A. C. Bode, W. J. P. van Enckevort, B. Kaptein, R. M. Kellogg, and E. Vlieg, Cryst. Growth Des. **8**, 1675 (2008); J. M. McBride and J. C. Tully, Nature (London) **452**, 161 (2008); M. Uwaha, J. Phys. Soc. Jpn. **77**, 083802 (2008); Y. Saito and H. Hyuga, *ibid.* **77**, 113001 (2008); H. Katsuno and M. Uwaha, J. Cryst. Growth **311**, 4265 (2009); M. Uwaha and H. Katsuno, J. Phys. Soc. Jpn. **78**, 023601 (2009); Z. El-Hachemi, J. Crusats, J. M. Ribó, and S. Veintemillas-Verdaguer, Cryst. Growth Design **9**, 4802 (2009); Y. Saito and H. Hyuga, J. Phys. Soc. Jpn. **78**, 104001 (2009); **79**, 083002 (2010); W. I. Noorduin, W. J. P. van Enckevort, H. Meekes, B. Kaptein, R. M. Kellog, J. C. Tully, J. M. McBride, and E. Vlieg, Angew. Chem. Int. Ed. **49**, 8435 (2010); H. W. Hatch, F. H. Stillinger, and P. G. Debenedetti, J. Chem. Phys. **133**, 224502 (2010); M. Uwaha, J. Cryst. Growth **318**, 89 (2011); Y. Saito and H. Hyuga, *ibid.* **318**, 93 (2011); J. A. D. Wattis, Orig. Life Evol. Biosph. **41**, 133 (2011); P. J. Skrdla, Cryst. Growth. Des. **11**, 1957 (2011); Z. El-Hachemi, J. Crusats, J. M. Ribó, J. M. McBride, and S. Veintemillas-Verdaguer, Angew. Chem. Int. Ed. **50**, 2359 (2011); H. Katsuno and M. Uwaha, Phys. Rev. E **86**, 051608 (2012).

[10] J. W. Gibbs, *Thermodynamics, Collected works, Vol. 1* (Yale University Press, New Haven, CT, 1948); M. Perez, Scr. Mater. **54**, 709 (2005).

[11] M. Iggland and M. Mazzotti, Cryst. Growth Des. **11**, 4611 (2011); CrystEngComm **15**, 2319 (2013).

[12] D. Gherase, D. Conroy, O. K. Matar, and D. G. Blackmond, Cryst. Growth Des. **14**, 928 (2014).

[13] See, e.g., M. J. Hounslow, R. L. Ryall, and V. R. Marshall, AIChE Journal **34**, 1821 (1988).

[14] C. Blanco, J. Crusats, Z. El-Hachemi, A. Moyano, S. Veintemillas-Verdaguer, D. Hochberg, and J. M. Ribó, ChemPhysChem **14**, 3982 (2013).

[15] D. Ramkrishna, *Population Balances: Theory and Applications to Particulate Systems in Engineering* (Academic, San Diego, 2000).

[16] Diffusive fluxes can also be accommodated in the PBE framework, and these arise when $\dot{\boldsymbol{X}}, \dot{\boldsymbol{R}}$ include stochastic processes [15].

[17] A. Mersmann, *Crystallization Technology Handbook*, 2nd ed. (Decker, New York, 2001).

[18] M. Stahl, B. Aslund, and A. C. Rasmuson, Ind. Eng. Chem. Res. **43**, 6694 (2004).

[19] M. Volmer, *Kinetik der Phasenbildung* (Steinkopff, Leipzig, 1939); D. Turnbull and J. C. Fisher, J. Chem. Phys. **17**, 71 (1949).

[20] J. W. Mullin, *Crystallization*, 4th ed. (Butterworths, Oxford, 2000).

[21] Polak and K. Sangwal, J. Cryst. Growth **152**, 182 (1995).

[22] J. A. D. Wattis, Physica D **222**, 1 (2006).

[23] $c(p,t)dp$ is the concentration of clusters made from p molecules in the range $(p, p+dp)$ at time t.

[24] P. L. Krapivsky, S. Redner, and E. Ben-Naim, *A Kinetic View of Statistical Physics* (Cambridge University Press, Cambridge, 2010).

[25] Numerical simulations of population balance equations typically require implementing some discretization scheme [15], and this step (say, via pivots [26]) leads one to deal with systems of coupled nonlinear ODEs. However, the continuum limit establishes that our kinetic scheme *is* a (microreversible) discrete version of these PBEs.

[26] S. Kumar and D. Ramkrishna, Chem. Eng. Sci. **51**, 1311 (1996); **51**, 1333 (1996); **52**, 4659 (1997).

[27] See Supplemental Material at http://link.aps.org/supplemental/10.1103/PhysRevE.91.022801 for simulations starting from initial enantiomeric excesses with the opposite sign to those employed in the main text.

[28] S. Qamar, A. Ahsfaq, I. Angelov, M. P. Elsner, G. Warnecke, and A. Seidel-Morgenstern, Chem. Eng. Sci. **63**, 1342 (2008).

[29] F. Czapla, H. Haida, M. P. Elsner, H. Lorenz, and A. Seidel-Morgenstern, Chem. Eng. Sci. **64**, 753 (2009).

[30] D. Hochberg and M.-P. Zorzano, Chem. Phys. Lett. **431**, 185 (2006).

[31] D. Hochberg and M.-P. Zorzano, Phys. Rev. E **76**, 021109 (2007).

[32] D. Hochberg, Phys. Rev. E **81**, 016106 (2010).